Journal of Manufacturing Engineering, June 2024, Vol. 19, Issue. 2, pp 057-066
DOI: https://doi.org/10.37255/jme.v19i2pp057-066

# EXPERIMENTAL INVESTIGATION OF MECHANICAL AND METALLURGICAL PROPERTIES IN FRICTION STIR SPOT WELDING OF DISSIMILAR AA6061-T6 TO COPPER

***Karimi Ivanaki M and Entezarian MM**

Department of Mechanical Engineering, University of Zanjan, Zanjan, Iran

## Abstract

In this study, the effects of important parameters of the FSSW process, rotational speed and dwell time, have been investigated on mechanical and metallurgical properties of dissimilar AA6061-T6 to the pure copper welded joint. In addition, the results were compared with the similar Al-Al and Cu-Cu welded joints. The results indicate that an increase in the rotational speed from 1250 to 1600 rpm and dwell time from 5 to 10 seconds improves the tensile and flexural strength of all the welded samples. Furthermore, at rotational speeds lower than 1250 rpm, due to reduced frictional heat generation, and above 1600 rpm, due to excessive heat production, the quality of the joints decreases. In this welding process, the amount of frictional heat generated directly affects the metallurgical structure, hardness of different welding zones, and intermetallic formations formed. The microstructure and the microhardness studies reveal that different welding parameters lead to the formation of fine grains and recrystallization in the stir zone and other regions with an increase in rotational speed and dwell time. This phenomenon is a result of the heat generated by friction and severe material deformation during welding. The refinement of grains contributes to increasing the hardness and strength. Moreover, the hardness analysis of the welded regions shows that the dissolution and growth of precipitates in the weld metal and its vicinity create a weaker region compared to the base metal, resulting in a decrease in hardness relative to the base metal.

***Keywords:*** *Friction Stir Spot Welding; Dissimilar Welding; Welding Parameters; AA6061-T6; Copper.*

## 1. Introduction

In recent years, reducing the weight of structural components to decrease fuel consumption and achieve higher efficiency is a fundamental and crucial challenge in transportation industries, particularly automotive and aerospace. The most important and fundamental suggestion for reducing the weight of vehicles is replacing heavy steel parts with lightweight alloys such as aluminium and copper [1]. In this regard, the use of dissimilar metals in conjunction with each other can lead to simultaneous use of the benefits of both metals. Joining, especially welding, of dissimilar materials has always been a major challenge in the industry [2]. The need to use materials with different properties alongside each other is felt in many industries. Among these materials, aluminium and copper can be mentioned, which are metals with unique properties and widely used in various industries.

In 2001, the automotive industry expanded the application of friction stir spot welding (FSSW) due to its special advantages, including low energy consumption and lower equipment costs compared to resistance welding [3]. FSSW is a method developed based on friction stir welding [4]. The creation of high-strength and fatigue-resistant joints with appropriate microstructure and hardness in common alloys such as aluminium and copper through fusion welding methods has been challenging and has limited the usability of these alloys [5]. Welding input parameters such as tool geometry, rotational speed, dwell time, axial force, and plunge depth usually influence grain flow and material distribution [6].

FSSW is a solid-state joining process in which first, a specially designed rotating tool enters the upper sheet, and then, due to the speed of rotation of the tool and the generation of frictional heat, the materials soften and undergo plastic deformation, finally creating a solid-state joint between the upper and lower sheet surfaces [7]. A schematic illustration of the FSSW process is shown in Fig. 1. This process consists of three stages: 1) tool plunge, 2) material mixing and stirring, and 3) tool withdrawal. The difference between FSW and FSSW lies in the tool's linear movement. In FSW, the tool has both rotational and linear motion after plunging into the surface. However, in FSSW, the tool is limited to

**Corresponding Author - E- mail: m.karimi@znu.ac.ir*

 

Journal of Manufacturing Engineering, June 2024, Vol. 19, Issue. 2, pp 057-066
DOI: https://doi.org/10.37255/jme.v19i2pp057-066

rotational motion only and does not have linear motion [8].

Improvement of mechanical and metallurgical properties, especially increasing strength, refinement of structure, and hardness of weld zones, has always been one of the most important challenges for researchers to achieve welded joints with minimal defects and the highest quality. Many researchers have investigated the mechanical and metallurgical properties of FSSW under the effects of multiple process parameters. Mehdi et al. [9] examined the effects of rotational speed and dwell time on strain rate, strength, grain refinement, and increased hardness of the weld zones for FSSW of dissimilar aluminium alloys. Zhang et al. [10] investigated the combined effects of rotational speed and plunge depth on the FSSW of AZ91 magnesium alloy. The results showed that plunge depth is the most effective parameter on weld quality, and an increase in rotational speed leads to higher strength of the welded samples.

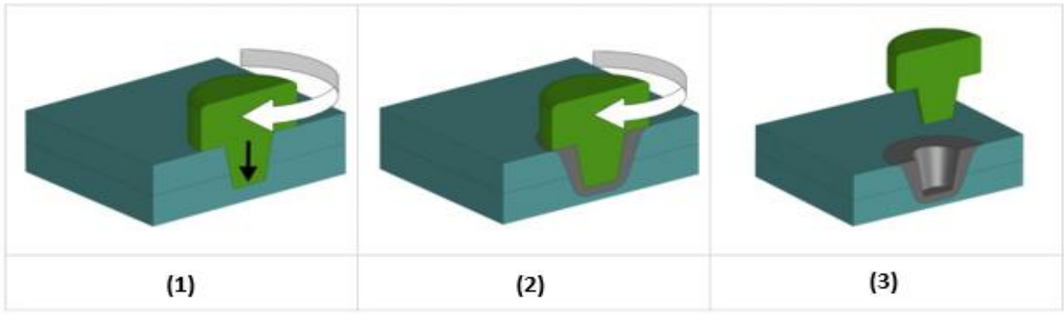


**Fig. 1 Schematic of the FSSW process [8]**

The first classification of the microstructure of FSSW was made by Treadwell [11], who reported that FSSW results in the formation of four microstructural zones: the base metal (BM), the heat-affected zone (HAZ), the thermomechanical affected zone (TMAZ), and the stir zone (SZ). Greg et al. [12] investigated the effects of process parameters such as rotational speed and dwell time on the strength of FSS welded AA6061 alloy and reported an increase in strength with the optimal values of these parameters. Patel et al. [13] studied the effect of rotational speed on the FSSW of aluminium sheets and found that increasing the rotational speed to an optimum value improves the microstructural properties and hardness of the weld spot. Zhang et al. [14] found that the intermetallic compound structure significantly influences the metallurgical properties of Al-Cu FSSW joints. The Al-Cu intermetallic combination helps to improve the refinement of the structure and increase the hardness of the joints. Ramkumar et al. [15] focused on the FSSW of AA2014 to AA6061 alloys and evaluated the effects of pin length, rotational speed variation, and dwell time on the weld zone strength. They reported that increasing pin length, rotational speed, and dwell time improves the weld strength. Akinlabi et al. [16] investigated the microstructure and fracture mechanisms of FS spot-welded AA5083 sheets. They concluded that the stir zone exhibited a much finer grain structure compared to other regions and had the highest hardness. The heat-affected zone (HAZ) and the thermomechanical-affected zone (TMAZ) have a lower hardness, and most of the fractures occurred in the common region between these two zones.

In this study, the mechanical and metallurgical properties of dissimilar Al-Cu welded samples were examined under the influence of various welding parameters. The effects of welding parameters on the mechanical strength and the hardness of the weld zones were investigated. Also, a comparison was made between these properties and the properties of similar Al-Al and Cu-Cu welded joints. In addition, the effect of the sheets positioning during the welding process of dissimilar Al-Cu on the mechanical properties of the joint was studied.

## 2. Research Methodology

In this study, FSSW was performed on 2 mm thick sheets of AA6061-T6 and pure commercial copper. The test specimens were prepared as rectangular plates with dimensions of 32 × 100 mm according to Fig. 2, and the surface area where the two sheets overlapped was determined as 32 × 35 mm2 for FSSW in the centre of this region.

Journal of Manufacturing Engineering, June 2024, Vol. 19, Issue. 2, pp 057-066
DOI: https://doi.org/10.37255/jme.v19i2pp057-066

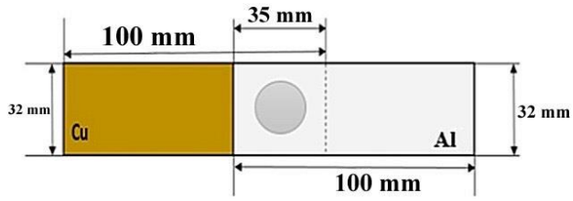


**Fig. 2 Geometric dimensions and test samples.**

It should be noted that before the welding process, the aluminium and copper sheets were first sanded to remove any contaminants and then cleaned with acetone. The mechanical properties and chemical compositions of the aluminium and copper alloys used in this study are reported in Tables 1 and 2, respectively.

**Table 1 Mechanical properties of AA6061-T6 and copper [17].**

| Elongation (%) | Ultimate tensile strength (MPa) | Yield strength (MPa) | Base Material |
|---|---|---|---|
| 8 | 201 | 222 | AA6061-T6 |
| 6.5 | 180 | 210 | Commercial Copper |

**Table 2 Chemical compositions of AA6061-T6 and Copper [18].**

| AA6061-T6 | | | | | | | | | |
|---|---|---|---|---|---|---|---|---|---|
| **Element** | **Al** | **Cr** | **Cu** | **Fe** | **Mg** | **Mn** | **Si** | **Ti** | **Zn** |
| % | 95.8 - 98.6 | 0.04 - 0.35 | 0.15 - 0.40 | 0.70 | 0.80 - 1.2 | 0.15 | 0.40 - 0.80 | 0.15 | 0.25 |
| Commercial copper | | | | | | | | | |
| Element | Cu | | | | | | | | |
| % | 100 | | | | | | | | |

For the welding process, the sheets were arranged in four positions as shown in Fig. 3: 1) aluminium sheet on the top and copper sheet at the bottom (position 1, Fig. 3a), 2) copper sheet on the top and aluminium sheet at the bottom (position 2, Fig. 3b), 3) similar Al-Al (position 3, Fig. 3c), and finally 4) similar Cu-Cu (position 4, Fig. 3d).

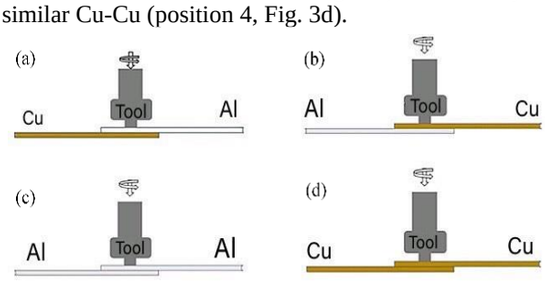


**Fig. 3 Different positions of AA6061-T6 and Cu during FSSW.**

The tool used for the FSSW process was made of H13 steel, which is the most common type of tool steel used in this welding process. After machining the tool, its hardness was increased from 15 RC to approximately 55 RC through heat treatment. In this study, a tool was used with a shoulder height and diameter of 30 mm and a pin with spiral threads with heights and diameters of 8.3 mm and 10 mm, respectively. The welding process was performed using a milling machine model FP4M. Due to the high force and torque applied to the welded parts during the process, the design and capability of the fixture are of great importance. Therefore, to hold the specimens securely during the process, a fixture and clamps were used, as shown in Fig. 4.

**Fig. 4 Fixtures and clamps for welding specimens.**

In order to perform the welding process, the tool dwell time ranged between 2 to 15 seconds, the tool plunge depth was 8.3 mm, and the rotational speed parameters of the tool were set to 500, 800, 1250, 1600, and 2000 rpm for the welded specimens in different positions. The appropriate parameters that resulted in the desired quality of the welded samples are presented in Table 3.

Journal of Manufacturing Engineering, June 2024, Vol. 19, Issue. 2, pp 057-066
DOI: https://doi.org/10.37255/jme.v19i2pp057-066

For the experimental evaluation of the tensile strength of the welded specimens, the tensile test was conducted according to ASTM-E8 standard [19] at room temperature with a strain rate of 2 mm/min. For this purpose, the specimens were prepared by cutting the wire perpendicular to the joint spot. Also, to measure the flexural strength of these specimens, the bending test was performed according to ASTM-E290 standard [20]. The dimensions of the flexural specimens were 6×20×200 mm in length, width, and thickness, respectively, and the distance between the support points from the centre of force application on both sides of the welding centre was 60 mm. The specimens under tension and flexural tests are illustrated in Fig. 5.

**Table 3 Optimal welding parameters for different sheets positioning.**

| No. | Sheets (position) | Rotational speed (rpm) | Dwell time (s) |
|---|---|---|---|
| 1 | Cu-Cu (4) | 1250 | 5 |
| 2 | Cu-Cu (4) | 1600 | 10 |
| 3 | Al-Al (3) | 1250 | 5 |
| 4 | Al-Al (3) | 1600 | 10 |
| 5 | Cu-Al (2) | 1250 | 5 |
| 6 | Cu-Al (2) | 1600 | 10 |
| 7 | Al-Cu (1) | 1250 | 5 |
| 8 | Al-Cu (1) | 1600 | 10 |

**Fig. 5 Tensile and flexural tests.**

To examine the microstructure of the welded specimens, the samples were cut perpendicular to the weld spot using the sectioning method and then mounted using a hot mounting press. Subsequently, the surface of the samples was ground using a belt polisher machine from Buehler, Germany, following the metallographic standard ASTM-E3 [21]. The microstructures of all the metallographic prepared samples were captured using a BMM-102 optical microscope from Nuvoc. In addition, SEM microstructure images were obtained using a Philips XL30 scanning electron microscope. The microhardness investigation of the welded sample regions was carried out using a Vickers microhardness tester, model FM-700, in accordance with ASTM-E384 hardness testing standard [22] with a 500gr load applied for 5 seconds on all samples.

## 3. Results and discussion

### 3.1. The Visual Appearance Quality

The tool rotational speed and the dwell time are some of the most influential parameters affecting the strength and the visual appearance of FSS welded specimens [23]. The effect of the tool rotational speed and the dwell time on the surface characteristics of the welds in different positions is shown in Fig. 6. And summarized in Table 3. By using the appropriate tool with the right parameters at rotational speeds of 1250 and 1600 rpm and dwell times of 5 and 10 seconds, the surface appearance of the welds is completely smooth and without any signs of distortions or other weld defects. It should be noted that changing the welding parameters, dwell time, and rotational speed has altered the surface appearance of the joints.

As the tool dwell time increases from 10 to 15 seconds and the rotational speed rises from 1600 to 2000 rpm, excessive softening and plasticization of the copper and aluminium sheet surfaces occur due to the increase of the frictional heat input, which leads to improper joint formation. Furthermore, at rotational speeds below 1250 rpm and the dwell times less than 10 seconds, suitable joint formation was not observed due to reduced heat generation.

### 3.2. The Tensile Test

The welded joints created by FSSW exhibit different mechanical properties and characteristics based on the selected welding parameters. In this study, various welding parameters were investigated in different positions to determine the appropriate conditions to achieve high-quality welds with optimal mechanical properties. The results of the tensile test are presented in Table 4.

Journal of Manufacturing Engineering, June 2024, Vol. 19, Issue. 2, pp 057-066
DOI: https://doi.org/10.37255/jme.v19i2pp057-066

**Fig. 6 Visual appearance of welded samples at different parameters.**

**Table 4 Tensile test results for the welded samples.**

| Sample No. | Yield strength | Ultimate tensile strength |
|---|---|---|
| 1 | 105 | 133 |
| 2 | 125 | 160 |
| 3 | 122 | 156 |
| 4 | 128 | 162 |
| 5 | 135 | 176 |
| 6 | 142 | 188 |
| 7 | 109 | 148 |
| 8 | 133 | 174 |

The results of the tensile test indicate that the strength values vary with changes in the welding parameters. In fact, these changes confirm that there is an optimal value for these parameters, above or below which the weld strength decreases. According to Table 4, increasing the welding parameters, the rotational speed from 1250 to 1600 rpm and the dwell time from 5 to 10 seconds leads to an increase in the yield and ultimate tensile strength values in all samples. In addition, the highest strengths were achieved when copper was on the top and aluminium at the bottom (position 2). Conversely, placing aluminium on the top and copper at the bottom (position 1) significantly reduced the strengths. Also, a decrease in the strength of the welded specimens was observed in all positions compared to the base metals.

Based on the applied tensile test on the welded samples, the fracture section of the weld can be categorized into three main types based on the mode and location of the fracture. In the first type, the weld nugget undergoes plastic deformation under tensile-shear forces and finally fractures from the weld nugget after elongation. Fig. 7 illustrates the deformation and eventual fracture of the weld nugget in the Cu-Al specimen (position 2).

**Fig. 7 Nugget fracture after high energy absorption.**

As shown in Fig. 8, the second type is characterized by shear fracture, where the weld fractures from the joint of the two sheets. It can be observed that optimal welding parameters can lead to improved weld quality and various fracture modes. According to Fig. 9, another type of fracture surface was observed in the weld joint, where the weld nugget experiences a rupture. It was observed that in some of the welded specimens, by keeping other parameters such as rotational speed and tool penetration depth constant, reducing the dwell time from 5 seconds to 10 seconds led to a decrease in the quality of the weld.

**Fig. 8 Shear failure of the weld at the joint interface of two sheets.**

**Fig. 9 Weld failure from the peripheral region around the nugget.**

### 3.3. Three-point bending test

In this study, a three-point bending test was used to measure the flexural strength of welded specimens with different welding parameters and positions. Fig. 10

Journal of Manufacturing Engineering, June 2024, Vol. 19, Issue. 2, pp 057-066
DOI: https://doi.org/10.37255/jme.v19i2pp057-066

shows the displacement results in the bending test. The results of the bending test indicate significant displacement in the welded specimens with the Cu positioned on the top (position 2). In addition, the flexural strengths of the Cu-Cu and Al-Al welded specimens are approximately equal under similar parameters, with no significant difference between them. However, the welding process has led to a reduction in their flexural strength. Furthermore, the displacement and force in the bending test were improved by increasing the welding parameters, the rotational speed and the dwell time in all-welded positions.

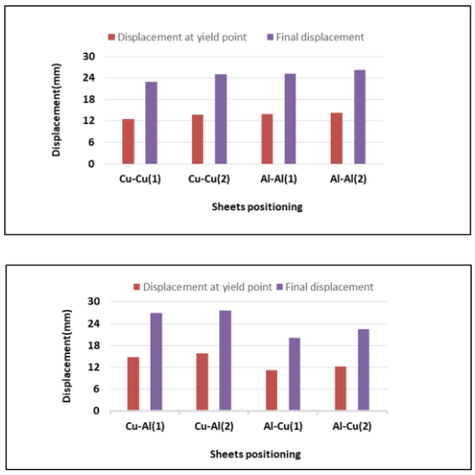


**Fig. 10 Samples were displaced under the bending test in different sheet positions.**

**Fig. 11 The appearance of the welded samples subjected to the bending test.**

Fig. 11 illustrates the visual appearance of the specimens subjected to the bending test. The results of the displacement variations presented in Fig. 10 also correspond well with the visual appearance of the bent specimens. As Fig. 11 presents, the welded sample with Cu on the top (position 2) exhibited better flexural strength, and no fracture was observed in this sample. The lowest values obtained from the bending test were related to the specimens with Al on the top (position 1), in which the welded joint has been fractured under the bending test.

### 3.4. Microhardness Testing

Fig. 12 illustrates hardness profiles for friction stir-welded samples of similar Cu-Cu and Al-Al in different welding parameters presented in Table 4. The results show that the hardness profiles are similar for all welded samples. Based on this profile, the hardness first decreased and then increased as it moved away from the centre of the weld zone towards the edge. These changes are related to the grain size based on the Hall-Petch relationship and the size of precipitates. In the weld zone, the grain size has decreased due to the phenomenon of dynamic recrystallization, and the precipitates have broken due to the rotation of the tool, transforming into fine precipitates. Both factors contribute to the increase in hardness in this region [24]. It is also worth noting that due to the difference in the rotational speed from the centre to the edges of the tool, a gradient in grain size is formed, which results in a difference in hardness between the edges and the centre. However, upon reaching the heat-affected zone where grain growth and precipitates occur, the hardness decreases significantly and then increases again upon reaching the base metal. In Fig. 12, the hardness profiles of the samples show that the hardness of the Cu-Cu and Al-Al samples rises with an increase in welding parameters, and the highest hardness value is observed in the welded Cu-Cu sample with the higher welding parameters.

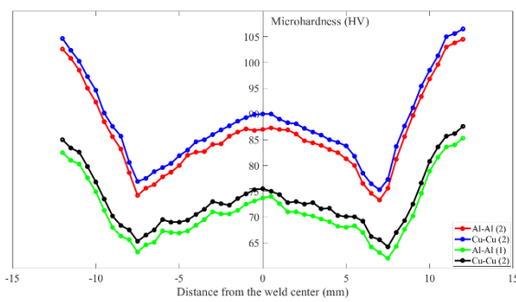


**Fig. 12 Micro hardness profile of Cu-Cu and Al-Al joints.**

A similar hardness profile was obtained for dissimilar Al-Cu and Cu-Al welded samples (Fig. 13). Based on this fig., the highest hardness belongs to the

Journal of Manufacturing Engineering, June 2024, Vol. 19, Issue. 2, pp 057-066
DOI: https://doi.org/10.37255/jme.v19i2pp057-066

welded sample with the higher welding parameters in which the copper was on the top (position 2), and vice versa, the lowest hardness goes to the welded sample with the lower welding parameters where the aluminium was on the top (position 1). In samples where aluminium was on the top (position 1), precipitation occurs in precipitation-hardened alloys such as AA6061-T6, resulting in very fine precipitates with small distances. They also act as obstacles to the movement of dislocations, thus increasing the strength of the material. In precipitation-hardened aluminium alloys, the hardness profile is strongly dependent on the distribution of precipitates and has little dependence on grain structure and dislocations [25]. In simpler terms, the low density of precipitates in the weld zone leads to a decrease in hardness compared to the base metal. Additionally, the material in the lower plate undergoes less deformation, which leads to coarser precipitates.

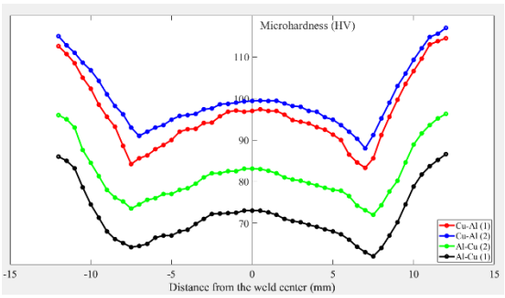


**Fig. 13 Micro hardness profile of Cu-Al and Al-Cu welded joints.**

### 3.5. Microstructure and Grain Size Study

The welding parameters affect changes in temperature, strain, strain rate, cooling and heating rate. All these factors also have an effect on the microstructural changes. Fig. 14 illustrates the macrostructure of sample no. 6 (Cu-Al), which includes different welding zones. As mentioned before, the weld zone can be divided into four regions, each with distinct microstructural characteristics [14, 26]. In Fig. 15, the microstructures of the welding zones are presented for sample no.6. Fig. 15(a) shows the microstructure of the aluminium base metal. Solid solution grains of the alpha phase, along with the distribution of insoluble intermetallic compounds in the aluminium base metal, are observed. The average grain size in the aluminium base metal was measured to be 4.11 µm using the ASTM method. Fig. 15(b) illustrates the microstructure of the copper base metal. Solid solution grains of copper containing twin regions in the base metal are detected. The average grain size in the copper base metal was measured to be 7.9 µm using the ASTM method.

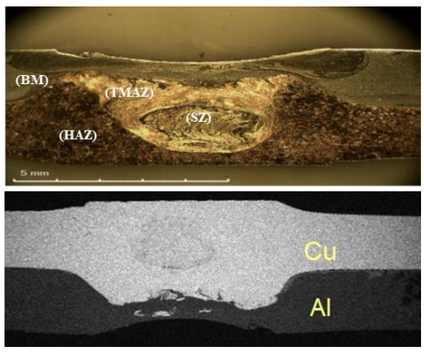


**Fig. 14 Macrostructure of different zones in FSSW welding.**

The microstructure of the nugget zone is shown in Fig. 15(c). This region is located just below the shoulder and in contact with the tool pin. Where severe plastic deformation and heat are generated by the tool-surface friction, resulting in dynamic recrystallization phenomena and the production of fine and equated grain structure. The average grain size in this region was measured to be approximately 4 µm, smaller than that of the base metal. The presence of a fine microstructure in the nugget zone leads to variation in hardness compared to other regions. In addition to grain size, precipitates also undergo changes in the nugget zone. The AA6061-T6 is typically artificially aged through heat treatment processes, containing precipitates of various sizes and shapes, including plate-like and needle-like structures, which significantly influence the metallurgical and mechanical properties such as hardness and strength [27]. These precipitates are composed of Mg2Si, and their size and distribution have a considerable impact on their material properties.

Fig. 15(d) displays the microstructure of the thermomechanical affected zone (TMAZ). In this region, materials undergo heat and deformation; however, the plastic strain is not sufficient for significant recrystallization to occur. Therefore, recrystallization either does not occur or is very limited. This region is a short and transient zone located at the boundary between the nugget zone and the heat-affected zone. It exhibits a structure with elongated grains oriented in the material flow direction, resulting from shear stress applied by the material flow.

Fig. 15(e) shows the microstructure of the heat-affected zone (HAZ), which is situated between the base metal and the thermomechanical-affected zone. This

Journal of Manufacturing Engineering, June 2024, Vol. 19, Issue. 2, pp 057-066
DOI: https://doi.org/10.37255/jme.v19i2pp057-066

region experiences only heat effects and does not undergo any deformation. Consequently, its structure appears similar to that of the base metal but with a larger grain size. It is noteworthy that the precipitates in this region are coarser than those in the base metal and nugget zone. This can be explained by the accelerated diffusion phenomenon and the absorption of alloying elements leading to precipitate growth with increasing temperature in this region.

As previously mentioned, an increase in rotational speed and dwell time leads to raised input heat and, consequently, elevated temperature. Therefore, it can be concluded that the welding parameter changes can also affect the structure of the weld regions. Grain size measurements in the nugget zone showed that at a consistent plunge depth of 0.3 mm, an increase in tool dwell time from 5 to 10 seconds, and rotational speed from 1250 to 1600 rpm, the grain size changed from 2.6 to 4 µm. Similarly, under the same parameters, the grain size in the heat-affected zone changed from 3.10 to 2.8 µm. A similar trend was observed in other welded samples. It should be noted that increasing these welding parameters resulted in a slight change in the grain size of the heat-affected zone, which can be attributed to the high thermal conductivity of aluminium and copper.

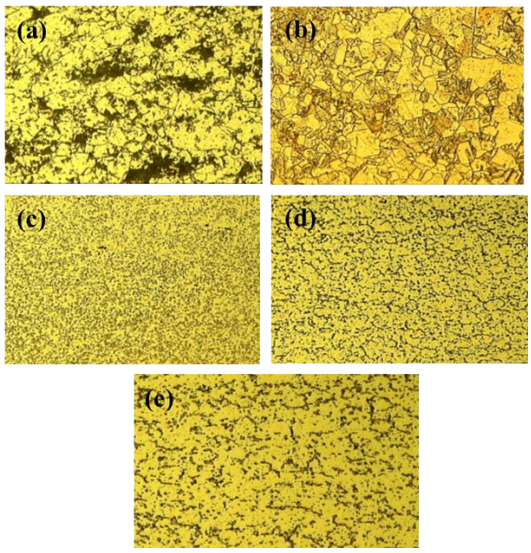


**Fig. 15 Different microstructural zones for sample 6 (Cu-Al). (a) Aluminium base metal; (b) Copper base metal; (c) Stir zone; (d) Thermomechanical affected zone; (e) Heat-affected zone.**

Fig. 16. Displays optical and electron microscopy images of the joint interface between the copper base metal and the weld zone (heat-affected zone). The phase changes, and extremely fine grain sizes at the joint interface between the nugget zone and the thermomechanical affected zone are clearly evident. This ultrafine microstructure significantly increases the hardness in the weld zone.

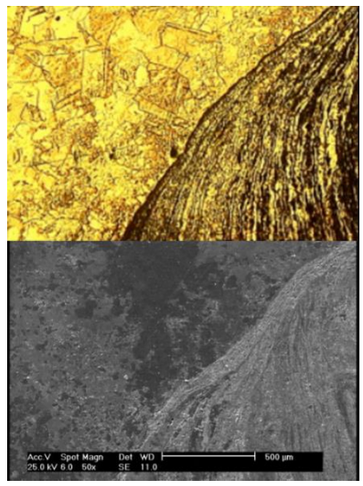

**Fig. 16 The joint interface of the copper base metal and the weld region**

## 4. Conclusion

In this study, the FSSW for dissimilar Al-Cu joints was done successfully using different welding parameters and positions. The optimal welding parameters were realized to achieve the welded joints with the appreciated appearance and good quality. The results show that the visual quality of the welded samples was satisfactory at optimal parameters of 1250 and 1600 rpm for rotational speed and 5 and 10 seconds for dwell time. The welded samples at lower rotational speeds below 1250 rpm and 5 seconds dwell time, as well as higher rotational speeds above 1600 rpm and 10 seconds dwell time, exhibited defects such as lack of fusion and excessive softening. In addition, the effects of the welding parameters and positioning were investigated on the mechanical strength of the welded joints and compared with similar Al-Al and Cu-Cu welded joints. The results indicate that increasing the rotational speed from 1250 to 1600 rpm and the dwell time from 5 to 10 seconds resulted in increased tensile strength, flexural strength, and hardness of the joints in all the welded samples. The highest tensile strength, flexural strength, and hardness were achieved when the copper was positioned on the top and the aluminium was at the bottom. In return, the lowest tensile and flexural strength

was obtained when the aluminium was on the top and the copper was at the bottom. The microstructure study shows that the metallurgical properties, particularly the microstructure, were significantly influenced by the FSSW process, leading to structural refinement and grain refinement compared to the base metals. In addition, the welding parameters play a significant role in grain size variations within the microstructure, where increasing these parameters resulted in finer grain structures in different welding zones.

## References

1. *M. M. Z. Ahmed, M. M. E.-S. Seleman, Z. A. Zidan, R. M. Ramadan, S. A. and N. A. Alsaleh, "Microstructure and Mechanical Properties of Dissimilar Friction Stir Welded AA2024-T4/AA7075-T6 T-Butt Joints," Metals, vol. 11, no. 1, p. 128, 2021. DOI: 10.3390/met11010128.*

2. *J. M. Piccini and H. G. Svoboda, "Effect of the Tool Penetration Depth in Friction Stir Spot Welding (FSSW) of Dissimilar Aluminium Alloys," Procedia Materials Science, vol. 9, pp. 868-877, 2015. DOI: 10.1016/j.mspro.2015.04.147.*

3. *K. Mehta and V. J. Badheka, "A review on dissimilar friction stir welding of copper to aluminium: Process, properties, and variants," Materials and Manufacturing Processes, vol. 31, no. 3, pp. 233-254, 2016. DOI: 10.1080/10426914.2015.1025971.*

4. *S. Dourandish, S. M. Mousavizade, H. R. Ezatpour, and G. R. Ebrahimi, "Microstructure, mechanical properties and failure behaviour of protrusion friction stir spot welded 2024 aluminium alloy sheets," Science and Technology of Welding and Joining, vol. 22, no. 4, pp. 295-307, 2017. DOI: 10.1080/13621718.2017.1386759.*

5. *H. A. Derazkola, H. Rahmani, M. Habibnia, and M. B. Limoie, "The feasibility study on AA7075 T-joint via friction stir welding process," Iranian Journal of Manufacturing Engineering, vol. 7, no. 1, pp. 21-32, 2016.*

6. *D. Zhang and T. Shibayanagi, "Material flow during friction stir spot welding of dissimilar Al2024/Al materials," Materials Science and Technology, vol. 31, no. 9, pp. 1077-1087, 2015. DOI: 10.1179/1743284714Y.0000000674.*

7. *N. Pathak, K. Bandyopadhyay, M. Sarangi, and S. K. Panda, "Microstructure and mechanical performance of friction stir spot-welded aluminum-5754 sheets," Journal of Materials Engineering and Performance, vol. 22, no. 1, pp. 131-144, 2013. DOI: 10.1007/s11665-012-0244-x.*

8. *M. Paidar, A. Khodabandeh, H. Najafi, and A. S. Rouh-aghdam, "Effects of the tool rotational speed and shoulder penetration depth on mechanical properties and failure modes of friction stir spot welds of aluminium 2024-T3 sheets," Journal of Mechanical Science and Technology, vol. 28, no. 12, pp. 4893-4898, 2014. DOI: 10.1007/s12206-014-1108-0.*

9. *H. Mehdi, R. S. Mishra, and S. M. Sharif, "Effect of multi-pass friction stir processing and SiC nanoparticles on microstructure and mechanical properties of AA6082-T6," Advances in Industrial and Manufacturing Engineering, vol. 3, pp. 1-14, 2021. DOI: 10.1016/j.aime.2021.100062.*

10. *H. Zhang et al., "Effect of tool plunge depth on the microstructure and fracture behaviour of refill friction stir spot welded AZ91 magnesium alloy joints," International Journal of Minerals, Metallurgy and Materials, vol. 27, no. 5, pp. 699-709, 2021. DOI: 10.1007/s12613-020-2044-x.*

11. *P. L. Threadgill, "Friction stir welds in aluminium alloys–preliminary microstructural assessment," TWI Bulletin, Mar./Apr. 2017.*

12. *Grag and A. Bhattachaty, "On lap shear strength of friction stir spot welded AA6061 alloy," Procedia Materials Science, vol. 10, pp. 203-215, 2017. DOI: 10.1016/j.jmapro.2017.02.019.*

13. *V. V. Patel et al., "Effect of tool rotation speed on friction stir spot welded AA5052-H32 and AA6082-T6 dissimilar aluminium alloys," Metallography, Microstructure, and Analysis, vol. 5, no. 2, pp. 142-148, 2016. DOI: 10.1007/s13632-016-0264-2.*

14. *M. Li, C. Zhang, D. Wang, L. Zhou, D. Wellmann, and Y. Tian, "Friction stir spot welding of aluminium and copper: a review," Materials, vol. 13, no. 1, p. 156, 2020. DOI: 10.3390/ma13010156.*

15. *T. Ramkumar et al., "Influence of rotation speeds on microstructure and mechanical properties of welded joints of friction stir welded AA2014-T6/AA6061-T6 alloys," Proceedings of the Institution of Mechanical Engineers, Part B: Journal of Engineering Manufacture, vol. 236, no. 8, pp. 9781-9791, 2022. DOI: 10.1177/09544089231188713.*

16. *E. T. Akinlabi, A. S. Osinubi, N. Madushele, S. A. Akinlabi, and O. M. Ikumapayi, "Data on microhardness and structural analysis of friction stir spot welded lap joints of AA5083-H116," Data in Brief, vol. 30, p. 106585, 2020. DOI: 10.1016/j.dib.2020.106585.*

17. *S. Venukumar, B. Baby, S. Muthukumaran, and S. V. Kailas, "Microstructural and Mechanical Properties of Walking Friction Stir Spot Welded AA 6061-T6 Sheets," Procedia Materials Science, vol. 5, pp. 656-665, 2014. DOI: 10.1016/j.mspro.2014.07.081.*

18. *V. V. Patel, D. J. Sejani, N. J. Patel, J. J. Vora, B. J. Gandhi, N. R. Padodara, and C. D. Vamja, "Effect of tool rotation speed on friction stir spot welded AA5052-H32 and AA6082-T6 dissimilar aluminium alloys," Metallography, Microstructure, and Analysis, vol. 5, no. 2, pp. 142-148, 2016.*

19. *ASTM-E8, Standard Mechanical testing and Evaluation Tensile testing, American Society for Testing and Material, 2000.*

20. *ASTM-E290, Standard test method for Bend testing of material for ductility, American Society for Testing and Material, 1998.*

21. *ASTM-E3, Standard guide for preparation of metallography specimen, American Society for Testing and Material, 2008.*

22. *ASTM-E384, Standard test method for micro-hardness of materials, American Society for Testing and Material, 2008.*

23. *M. Bilici and F. Hunt, "The optimisation of welding parameters for friction spot welding of high density polyethylene sheets," Materials and Design, vol. 32, no. 7, pp. 4074-4079, 2011. DOI: 10.1016/j.matdes.2011.03.014.*

24. *Y. Tozaki, Y. Uematsu, and K. Tokaji, "Effect of tool geometry on microstructure and static strength in friction stir spot welded aluminum alloys," International Journal of Machine Tools and Manufacture, vol. 47, no. 15, pp. 2230-2236, 2007. DOI: 10.1016/j.ijmachtools.2007.07.005.*

25. *V. X. Tran, J. Pan, and T. Pan, "Effects of processing time on strengths and failure modes of dissimilar spot friction welds between aluminum 5754-O and 7075-T6 sheets," Journal of Materials Processing Technology, vol. 209, no. 8, pp. 3724-3739, 2009. DOI: 10.1016/j.jmatprotec.2008.08.028.*

26. *Z. Zhang, X. Yang, J. Zhang, G. Zhou, X. Xu, and B. Zou, "Effect of welding parameters on microstructure and mechanical properties of friction stir spot welded 5052 aluminum alloy," Materials and Design, vol. 32, no. 8, pp. 4461-4470, 2011. DOI: 10.1016/j.matdes.2011.03.058.*

27. *P. Prangnell and D. Baklavas, "Novel Approaches to Friction Spot Welding Thin Aluminum Automotive Sheet," Materials Science Forum, vol. 638-642, pp. 1237-1242, 2010. DOI: 10.4028/www.scientific.net/MSF.638-642.123*